Evidence for the co-existence of isomers of water dimer radical cations and their inter-conversion in a linear ion trap

Xinglei Zhang, Yunpeng Zhang, Xin Zhou, Junqiang Xu, Dongbo Mi [*]

Jiangxi Key Laboratory for Mass Spectrometry and Instrumentation, East China University of Technology, Nanchang, 330013, China

ARTICLE INFO

ABSTRACT

Water dimer radical cations are regarded as key intermediates in many aqueous reactions and biochemical processes. However, the structure of the water dimer radical cations, and particularly the inter-conversion between their isomers, remain difficult to investigate experimentally due to their short lifetime and low abundance under ambient conditions. Furthermore, the isomers cannot be distinguished in a full mass spectra. In this study, we report the experimental evidence for the hemi-bonded and proton-transferred isomers of gas-phase water dimer radical cations, and the inter-conversion process between them in a linear ion trap at low pressure and near room temperature. Multiple collisions of isolated water dimer radical cations with He inside the ion trap were systematically investigated; first, under different trapping times (i.e., reaction times) ranging from 0.03 to 800 ms, and then at a very low collision energies ranging from 0.1% to 10% normalized collision energy. The proton-transferred isomers were dominant at shorter trapping times (≤ 250 ms), while the hemi-bonded isomers were dominant at longer trapping times (250−800 ms). Moreover, the difference in symmetry of the shapes of the $H_2O^{\bullet+}$ signal profiles and the H_3O^+ signal profiles implied the existence of two kinds of isomers and there were small potential differences between them. Our results also suggested that by tuning the experimental parameters the hemi-bonded isomers would become dominant, which could allow the study of novel chemical reactions involving the hemi-bonded two-center-three-electron (2c-3e) structure in a linear ion trap.

1. Introduction

The study of various variants of water molecules, such as micro-droplets, the protonated water clusters, and hydrated electrons, has become a field of research that provides surprising research outcomes [1–7]. As an important intermediate in radiation chemistry and radio-biology, the water radical cations, $(H_2O)_n^{\bullet+}$, have attracted much attention for their role in reactions, both experimentally and theoretically [8,9]. However, there have been few reports of inter-molecular interactions of $(H_2O)_n^{\bullet+}$ due to its high reactivity [9]. With the rapid development of quantum chemical theory in cluster ion structures [10], bonding properties [11], and dynamic simulations of reactions [12], great theoretical progress has been made in determining the formation mechanism of $(H_2O)_n^{\bullet+}$. Recently, as well documented [13,14], water radical cations were naturally abundant in pure bulk water, which indicates that a water radical cation/anion pair ($H_2O \cdots OH_2 \rightleftharpoons H_2O^{\bullet+} + H_2O^{\bullet-}$) has been formed based on hydrogen bond-induced electron transfer. Currently, there are two main methods for forming $(H_2O)_n^{\bullet+}$. On one hand, $(H_2O)_n^{\bullet+}$ could be generated through the ionization of water due to the strong

---

* Corresponding author.
E-mail address: wjmdb@hotmail.com (D. Mi).

electric field at the micro-droplet interface [15]. On the other hand, $(H_2O)_n^{\bullet+}$ could be generated in water vapor plasma, which is produced under mild corona discharge [16], which provides a facile approach to access the high reactivity of water radical cations under ambient conditions [17,18].

Studies of the water dimer radical cation, $(H_2O)_2^{\bullet+}$, by means of quantum chemical and molecular dynamics methods are of considerable interest [19,20]. The simulation results for the structural properties of $(H_2O)_2^{\bullet+}$ based on *ab*-initio, semi-empirical, and density functional theory calculations are consistent, with two stationary points found to be the local minima: the proton-transferred isomer with $[H_3O^+ \dots {}^\bullet OH]$ characteristics and the hemi-bonded isomer with $[H_2O \cdots OH_2]^{\bullet+}$ characteristics [10,12,21]. Taking the results at the aug-cc-PVQZ CCSD(T) level as an example, these two isomers are separated by 8.8 kcal/mol with an inter-conversion barrier of 15.1 kcal/mol [10], and the proton-transferred isomer with the ion-radical structure is the minimum energy arrangement [22].

In addition to the theoretical simulations, only a few reports have provided experimental evidence for the structural properties of $(H_2O)_2^{\bullet+}$. Collision studies of the $(H_2O)_2^{\bullet+}$ ion in the gas phase are more consistent with the proton-transferred structure [23]. Gardenier et al. [19] showed the infrared (IR) spectra of $Ar \bullet (H_2O)_2^{\bullet+}$ and $(H_2O)_2^{\bullet+}$, in which a strong triplet approximately at 2000 cm^{-1} could be clearly detected and attributed to the bridging proton of the proton-transferred isomer. They argued that the hemi-bonded isomer had no contribution to the spectra [19]. Through a direct oxygen … oxygen bond contraction, a transient radical cation complex, abbreviated as $\bullet OH(H_3O^+)$, was formed within 140 fs and captured by Lin et al. [24]. The radical cation complex was confirmed as the intermediate complex for the proton transfer between $H_2O^{\bullet+}$ and H_2O, which was consistent with the proton-transferred isomers of $(H_2O)_2^{\bullet+}$.

Until recently, the hemi-bonded isomer of $(H_2O)_2^{\bullet+}$ has been poorly understood. It is interesting to note that in the collision induced dissociation (CID) experiments of thermalized water dimer radical cations reported by Nibbering et al. [25], there was a substantial yield of $H_2O^{\bullet+}$, indicating the hemi-bonded motif of $(H_2O)_2^{\bullet+}$. Collision reactions of $(H_2O)_2^{\bullet+}$ in a single collision with D_2O in a collision cell at low pressure were investigated at a very low collision energy, ranging from 0.05 to 2.0 eV, using a guided-ion beam tandem mass spectrometer (MS^n, n ≥ 2). Only the $H_2O^{\bullet+}$ fragment, and not the H_3O^+ fragment, was observed, which indicated that the hemi-bonded isomer was dominant, as opposed to the proton-transferred isomer [26].

The two structural motifs may be formed depending on how the water dimer radical cations are generated in the ion source. Recently, Wang et al. [16]computationally and experimentally confirmed the existence of two isomers of $(H_2O)_2^{\bullet+}$. Later, the structure of $(H_2O)_2^{\bullet+}$ was further studied by Li et al. [27] in a CID experiment using an isotope labeling method. The dissociation (CID) results showed that two kinds of fragment ions of *m/z* 19 (H_3O^+) and *m/z* 18 ($H_2O^{\bullet+}$) could be competitively generated by loss of ●OH and H_2O, respectively, indicating the two different isomers of $(H_2O)_2^{\bullet+}$. The CID with isotope labeling results indicated that $(D_2O)_2^{\bullet+}$, $(H_2O \bullet D_2O)^{\bullet+}$, and $(H_2O \bullet H_2^{18}O)^{\bullet+}$ also exist as proton-transferred and hemi-bonded isomers.

In our previous reports, indirect evidence indicated the co-existence of the proton-transferred and hemi-bonded isomers of the water dimer radical cations in the reactions between $(H_2O)_2^{\bullet+}$and benzene. Protonated benzene cations (*m/z* 79) [28] and protonated phenol cations (*m/z* 95) [17] could be formed from the $[H_3O^+ \dots {}^\bullet OH]$ isomer or even from their respective dissociation products: H_3O^+ or $^\bullet OH$. Alternatively, the abundance of benzene radical cations (*m/z* 78) [28] as well as the phenol radical cations (*m/z* 94) could have originated from the $[H_2O \cdots OH_2]^{\bullet+}$ isomer, with the latter case being consistent with the conclusions of Qiu et al. [15].

Until recently, the inter-conversion between the protonated isomer and hemi-bonded isomer lacked experimental evidence, and was based on only a theoretical analysis [10]. The unique formation of hemi-bonded isomers has restricted in-depth research on the structure-property relationship of water radical cations, which would enable a better understanding of the mechanism of natural processes and the discovery of novel gas phase reactions. Both products resulting from the reaction with $[H_2O \cdots OH_2]^{\bullet+}$ and $[H_3O^+ \dots {}^\bullet OH]$ could be detected under ambient conditions in the ion source. In this study, the inter-conversion of the two isomers of $(H_2O)_2^{\bullet+}$ in a linear ion trap at low pressure and near room temperature was achieved for the first time. Most importantly, our results suggest that the hemi-bonded isomers could be dominant in the gas phase under suitable conditions, providing a new method for preparing highly reactive hemi-bonded isomers and studying the novel chemical reactions exclusively induced by them.

2. Experimental section

Mass spectrometry (MS) experiments were conducted using a commercial linear ion trap mass spectrometer (LTQ-XL, Thermo-Fisher, San Jose, CA, USA). The mass spectrometer was coupled with a closed, home-built ambient corona discharge ion source. Details of the ion source can be found in previous reports from our laboratory [17,18]. Briefly, as shown in Fig. S1, a stainless-steel discharge needle with an outer diameter (OD) of 150 μm, sharp tip (curvature radius 7.5 μm) and an insulator on the back end was fixed co-axially with two fused silica capillaries using ferrules [17,18]. Ultra-pure water, which was not used in this work, could be introduced through the inner fused silica capillary (ID 0.25 mm, OD 0.40 mm). The carrier gas (Ar with high purity, 99.999%, 0.3 MPa), which contained no more than 1 ppm water vapor, was introduced through the outer fused silica capillary (ID 0.53 mm) at a flow rate of 20 mL/min [17,18]. The tip of the inner capillary orifice protruded approximately 0.5 mm out of the outer capillary orifice and the tip of the discharge needle protruded about 0.5 mm out of the inner capillary orifice. The distance from the tip of the discharge needle to the inlet capillary of the mass spectrometer was approximately 22 mm [17,18].

Mass spectra were collected in the mass-to-charge (*m/z*) range of 15–200. The capillary voltage was 1.0 V. The tube lens voltage was 0.0 V. Because the temperature could affect the stability of the generated $(H_2O)_2^{\bullet+}$ during the process for transferring ions to the detector, the ion capillary temperature was set to be 150 °C, enabling the intensity of $(H_2O)_2^{\bullet+}$ to reach a maximum [16,17]. The temperature in the trap was near room temperature as discussed in our previous report [18]. The carrier gas was introduced into the closed ion source for 20−30 min to completely replace the remaining gas with high-purity Ar. Experiments were conducted in positive

ion detection mode (+2.5 kV). The water vapor, as the trace impurity in the carrier gas, was then ionized. Other parameters were set to default instrument values without any further optimization. The background neutrals inside the trap were continuously renewed through vacuum pumping. High-purity He gas (99.999%) was introduced to maintain the vacuum in the ion trap at about 1×10^{-5} Torr [18] based on the vacuum gauge reading. The injected He was used as collision gas and a unique dissociation would occur when the isolated ions were exposed to the He atoms.

3. Results and discussion

As shown in Fig. S2, water radical cations, $(H_2O)_2^{\bullet+}$ (m/z 36) and $(H_2O)_3^{\bullet+}$ (m/z 54), and protonated water clusters, $H^+(H_2O)_2$ (m/z 37) and $H^+(H_2O)_3$ (m/z 55) were detected as the major species generated upon the ambient corona discharge of water vapor in Ar [18]. Consistent with our earlier experiments under similar ionization conditions [16], these signals attributed to the above ions were further confirmed by using isotopically labeled water. The choice of the inert gas had little effect on the generation of the water radical cations as well as the protonated water clusters, which we reported previously [16], indicating that the $(H_2O)_2^{\bullet+}$ could be generated when suitable amounts of energy were deposited into pure water vapor under atmospheric pressure, rather than reactions between inert gas ions and water molecules.

To investigate the isomer structures of $(H_2O)_2^{\bullet+}$, the generated $(H_2O)_2^{\bullet+}$ could be trapped in the linear ion trap and the fragment ions could be detected based on the multiple collisions with He atoms. Because the H_3O^+ ions were the fragment ions of both the $(H_2O)_2^{\bullet+}$ and the $H^+(H_2O)_2$ ions, it would be beneficial to study the trend of ion intensity of $H^+(H_2O)_2$ simultaneously when studying the inter-conversion between the two isomers of $(H_2O)_2^{\bullet+}$. We therefore trapped $H^+(H_2O)_2$ alone or both the $(H_2O)_2^{\bullet+}$ and $H^+(H_2O)_2$ in the linear ion trap. However, the intensity of $(H_2O)_2^{\bullet+}$ trapped in the linear ion trap (Fig. S3) was significantly reduced compared with the intensity detected in the full scan (Fig. S2). The $(H_2O)_2^{\bullet+}$ that remained in the trap should possess the most thermodynamic stable structure, indicating that most of the $(H_2O)_2^{\bullet+}$ isolated in the trap was the proton-transferred isomer. We speculated that most of the $(H_2O)_2^{\bullet+}$, especially the hemi-bonded isomers, generated in the water/Ar plasma was unstable when trapped and could be dissociated before being transferred to the detector. This would be a reasonable explanation for the phenomenon discussed above, in which most of the $(H_2O)_2^{\bullet+}$ generated in the ion source was lost during the trapping process.

First, $H^+(H_2O)_2$ alone was trapped in the linear ion trap. The signal intensities for H_3O^+ and $H^+(H_2O)_2$ in the linear ion trap as a function of trapping time are shown in Fig. 1 at 0% normalized collision energy (NCE%). No $H_2O^{\bullet+}$ (m/z 18) was detected in the ion trap and only small amounts of H_3O^+ (m/z 19) were detected. Moreover, the ion intensity of H_3O^+ was almost constant as the trapping time increased from 0.03 up to 800 ms. In contrast, a clear decrease in the ion intensities of $H^+(H_2O)_2$ at a trapping time around 250−300 ms was detected. We assumed that the H_3O^+ observed here would not be attributed to the dissociation of $H^+(H_2O)_2$. However, the background signals appeared to leak into the ion trap. It would be interesting to investigate the reasons for the decrease in ion intensity of $H^+(H_2O)_2$ in the trap. We attributed this phenomenon to two possible reasons. 1) As is well documented [29–31], the ions with low m/z, especially close to the detection limit of the ion trap, such as $(H_2O)_2^{\bullet+}$, and $H^+(H_2O)_2$, can be easily ejected out of the ion trap. Thus, we speculated that the decrease in the ion intensity of $H^+(H_2O)_2$ could be partially caused by the ion resonance ejection of the translational hot ions after trapping up to 250 ms. 2) We attributed the sudden decrease of $H^+(H_2O)_2$ after 250 ms to the fact that an equilibrium between $H^+(H_2O)_2$ and $H^+(H_2O)_2 \bullet H_2$ was achieved, which means parts of the $H^+(H_2O)_2$ ions would be converted to the protonated water-hydrogen clusters, which was consistent with our previous report [18](as shown in Scheme 1a).

Then, $(H_2O)_2^{\bullet+}$, along with $H^+(H_2O)_2$, was trapped in the linear ion trap at 0% NCE% (Fig. 2). As $(H_2O)_2^{\bullet+}$ was trapped in the linear ion trap from 0.03 to 250 ms, the ion intensities indicated that $(H_2O)_2^{\bullet+}$ exhibited an obvious dissociation, and the contribution of $H^+(H_2O)_2$ to the fragment ions generated in the ion trap was limited (the same as shown in Fig. 1). As mentioned above, the decrease in the ion intensity of $(H_2O)_2^{\bullet+}$ around this time was caused mainly by the dissociation, but was partially due to the ion ejection. Two kinds
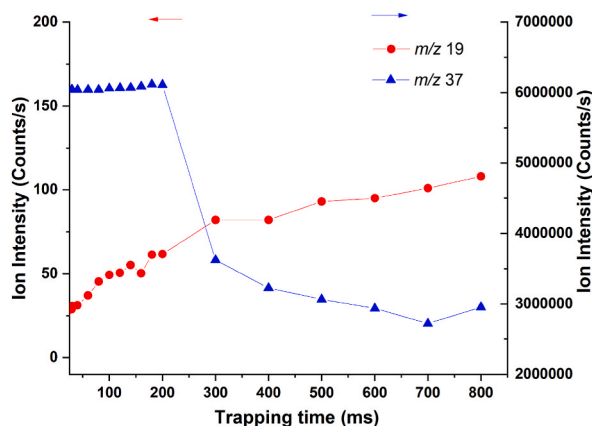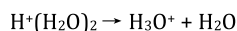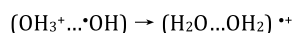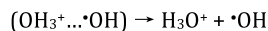

Fig. 1. Signal intensities for H_3O^+ (m/z 19, red circles) and $H^+(H_2O)_2$ (m/z 37, blue triangles), trapped in the linear ion trap as a function of the trapping time of $H^+(H_2O)_2$ ions. (Note: *there is no scaling of m/z 37 in this plot and each curve represents the average of three groups of parallel experiments*). (For interpretation of the references to colour in this figure legend, the reader is referred to the Web version of this article.)

$$H^+(H_2O)_2 + H_2 \leftrightarrows H^+(H_2O)_2 \bullet H_2$$

$$(H_2O...OH_2)^{\bullet+} \rightarrow H_2O^{\bullet+} + H_2O$$

$$(OH_3^+...^\bullet OH) \rightarrow H_3O^+ + {}^\bullet OH$$

$$(OH_3^+...^\bullet OH) \rightarrow (H_2O...OH_2)^{\bullet+}$$

$$H^+(H_2O)_2 \rightarrow H_3O^+ + H_2O$$
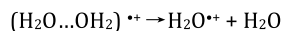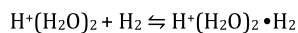
Scheme 1. A scheme illustrating the dissociation/fragmentation and conversions of water radical cations as well as protonated water clusters.
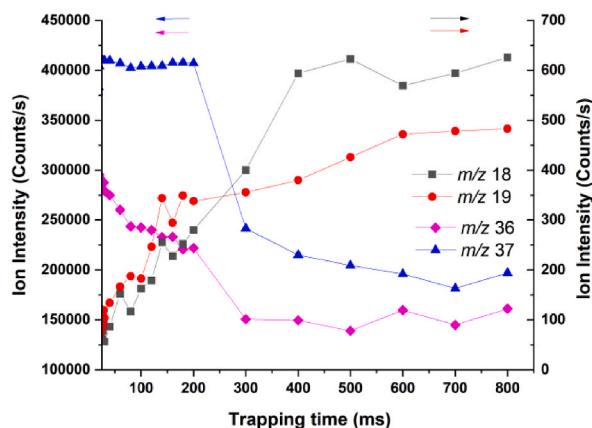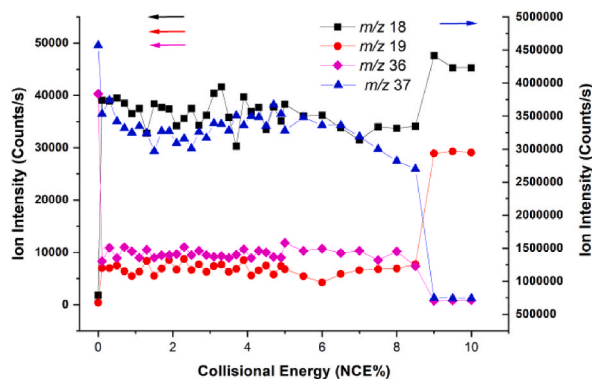

Fig. 2. Signal intensities for $H_2O^{\bullet+}$ (*m/z* 18, black squares), H_3O^+ (*m/z* 19, red circles), $(H_2O)_2^{\bullet+}$ (*m/z* 36, magenta rhombuses), and $H^+(H_2O)_2$ (*m/z* 37, blue triangles), isolated in the linear ion trap as a function of the trapping time of $(H_2O)_2^{\bullet+}$ ions. (Note: *for comparison, the ion intensity of the m/z 37 ions in this figure is one-fifteenth of the absolute ion intensity. Each curve represents the average of three groups of parallel experiments.*). (For interpretation of the references to colour in this figure legend, the reader is referred to the Web version of this article.)

of fragment ions were detected: $H_2O^{\bullet+}$ (*m/z* 18), accompanied by H_3O^+ (*m/z* 19), which was formed following the loss of H_2O from hemi-bonded isomers (as shown in Scheme 1b); and the ●OH radical from proton-transferred isomers (as shown in Scheme 1c), which was consistent with our previous report [27]. The ion intensities of the fragment ions showed that the intensity of proton-transferred isomers exceeded that of the hemi-bonded isomers, which was consistent with previous speculation. However, the ratio of the intensity of $H_2O^{\bullet+}$ to the intensity of H_3O^+ still increased during this time (Fig. 2 and Figs. S3a–c), suggesting that parts of the proton-transferred isomers were converted to hemi-bonded isomers (as shown in Scheme 1d). With the trapping of $(H_2O)_2^{\bullet+}$ up to 400.03 ms (Fig. 2 and Fig. S3d), the fragment ions of the hemi-bonded isomers became the dominant ions.

Next, the $(H_2O)_2^{\bullet+}$ that had been trapped in the linear ion trap up to 800 ms was further exposed to He atoms with increasing collision energies, from 0% to 0.1% NCE%, and eventually up to 10% NCE% (Fig. 3). Further experimental evidence for the inter-

Fig. 3. Signal intensities for $H_2O^{\bullet+}$ (*m/z* 18, black squares), H_3O^+ (*m/z* 19, red circles), $(H_2O)_2^{\bullet+}$ (*m/z* 36, magenta rhombuses), and $H^+(H_2O)_2$ (*m/z* 37, blue triangles), isolated in the linear ion trap as a function of the normalized collision energy. (Note: *there is no scaling of m/z 37 in this plot and each curve represents the average of three groups of parallel experiments.*). (For interpretation of the references to colour in this figure legend, the reader is referred to the Web version of this article.)
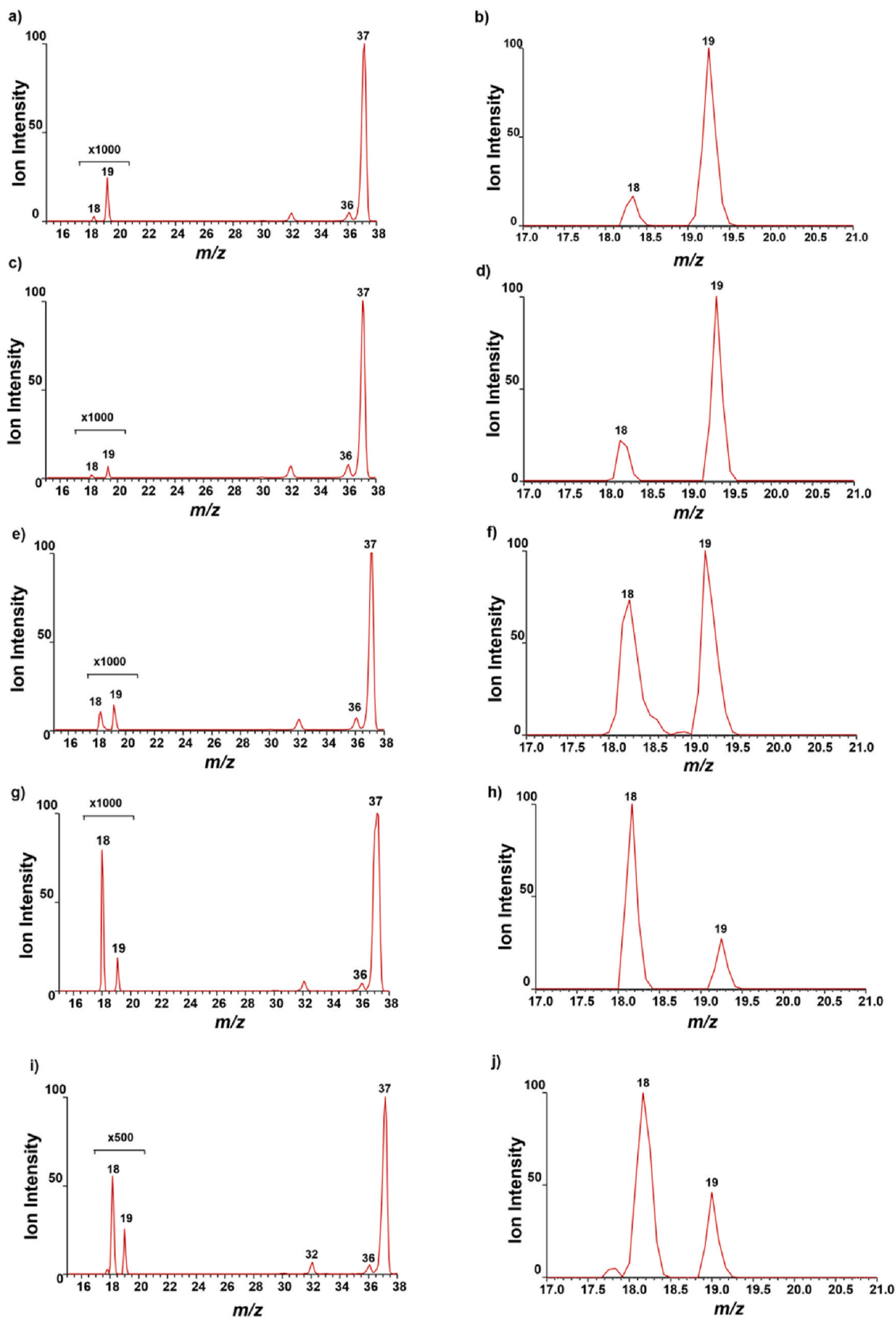
(caption on next page)

Fig. 4. Peak profiles for the mass spectra measured under different trapping times: (a, b) 0.33 ms, (c, d) 3.03 ms, (e, f) 30.03 ms, (g, h) 400.03 ms, and (i, j) 800.03 ms. (Note: *The unavoidable signals at m/z at* 32 *might be assigned to* $O_2^{\bullet+}$).

conversion between these isomers could be detected from the ion intensity trends of their fragment ions. Depositing a small amount of extra energy into $(H_2O)_2^{\bullet+}$ resulted in a significant decrease in the ion intensity of $(H_2O)_2^{\bullet+}$, which was associated with the increase of its fragment ion, $H_2O^{\bullet+}$ (Fig. 3 and Figs. S4a–c). We attributed this to the dissociation of the hemi-bonded isomer of $(H_2O)_2^{\bullet+}$ formed in the linear ion trap (similar to Scheme 1b). It was clear that most of the $(H_2O)_2^{\bullet+}$ was dissociated during this process. However, only some parts of the trapped $H^+(H_2O)_2$ was dissociated, and a slight increase in the amount of fragment ions, H_3O^+, could be detected (as shown in Scheme 1e). The generated fragment ions, H_3O^+, were obviously caused by the dissociation of $H^+(H_2O)_2$ because the proton-transferred isomer of $(H_2O)_2^{\bullet+}$ had already been consumed. Furthermore, the decrease of $H^+(H_2O)_2$ was much lower than that of $(H_2O)_2^{\bullet+}$, due to the higher binding energy in the $H^+(H_2O)_2$ ions. This was consistent with previous reports that the binding energy of the water dimer radical cation was only 75% of that of the protonated water dimer cluster [32–34].

As the collision energy continuously increased up to 9% NCE% (Fig. 3 and Fig. S4c), the multiple collision energy was large enough to produce a significant dissociation of $H^+(H_2O)_2$, accompanied by a sharp increase in its fragmentation ions, H_3O^+(the same as in Scheme 1e). Simultaneously, the small amount of $(H_2O)_2^{\bullet+}$ remaining in the trap was almost completely fragmented with an observed increase of its fragmentation ions, $H_2O^{\bullet+}$(the same as in Scheme 1b). The residual $H^+(H_2O)_2$ isolated in the ion trap was further fragmented as the collision energy increased up to 20% NCE% (Fig. S4d).

For mass analyzer CID, the normalized collision energy is a measure of the amplitude of the resonance excitation radio frequency (RF) voltage applied to the end-caps. The normalized collision energy scales the amplitude of the voltage to the parent mass. The equation for calculating the amplitude of the resonance excitation RF voltage is as follows:

$$\text{Amplitude} = \text{NCE\%} \ / 30\% \ \{\text{parent mass} \times \text{tick amp slope} + \text{tick amp intercept}\} \tag{1}$$

where *NCE%* is the normalized collision energy and *tick amp* is the amplitude of the resonance excitation RF voltage. The calculated results for the energy of single collisions with NCE% set as 0.1%, 5%, and 10% are listed in Table S1. These values were much lower than the bond energy for $(H_2O)_2^{\bullet+}$ [35] and we therefore postulated that the dissociation of $(H_2O)_2^{\bullet+}$ in the linear ion trap was promoted through multiple collisions with He atoms.

As an additional observation, the resolution (m/∆m) of the fragment ion at *m/z* 18 was obviously poorer than the other fragment ion at *m/z* 19 because an asymmetry in the shape of the $H_2O^{\bullet+}$ signal profiles was detected (Fig. 4 a–f), which tailed to the higher mass region. The shorter the trapping time of $(H_2O)_2^{\bullet+}$ in the linear ion trap, the more obvious the asymmetry of the shape. In contrast, the shape of the H_3O^+ signal was much more symmetrical.

It could be inferred that the fragment ions of proton-transferred isomers of $(H_2O)_2^{\bullet+}$ (*m/z* 36) had been generated mainly in the ion trap during the collision-induced dissociation. Because the $[H_3O^+ \ldots \bullet OH]$ structure possessed a better stability than the $[H_2O \cdots OH_2]^{\bullet+}$ structure, the proton-transferred isomers would not have been dissociated within the period of ion transfer to the detector. In contrast, it could be inferred that most of the hemi-bonded isomers were fragmented in the ion trap during the multiple collisions with the He atoms, while some parts of the relatively unstable hemi-bonded isomers were dissociated into the fragment ions during the period of ion transfer to the detector, resulting in a broadened kinetic energy distribution and consequently broadened mass spectral peaks [35,36]. As the trapping time extended (Fig. 4 g–j), taking 800 ms as an example, most of the dissociation of the hemi-bonded isomers could occur in the ion trap, and the ratio of the fragment ions of hemi-bonded isomers generated during the period of ion transfer to the detector was substantially reduced, which led to more symmetrical $H_2O^{\bullet+}$ (*m/z* 18) signal profiles. A methodological flow chart (Fig. S5) is presented in the supporting information to show the intrinsic correlation between the figures discussed above.

4. Conclusions

Our results suggest a novel method to study the structural properties of water dimer radical cations based on CID in a linear ion trap mass spectrometer at low pressure. The experimental data indicated that, in addition to proton-transferred isomers, hemi-bonded isomers contribute to the $(H_2O)_2^{\bullet+}$ signal in the gas phase. The data also indicated an inter-conversion between these isomers. Our results further suggest that by tuning experimental parameters, such as the trapping time or collision energy, the gas-phase water dimer radical cations would be dominated by hemi-bonded isomers. However, the loss of water dimer radical cations during the trapping process still needs to be overcome. The method developed here allows the study of novel chemical reactions involving hemi-bonded two-center-three-electron (2c-3e) isomers in a linear ion trap. The other reactants, such as gas reactants or volatile organic compounds, could be introduced into the ion trap with He gas and then the reaction would occur. This is an interesting topic for future research.

Author contribution statement

Xinglei Zhang: Performed the experiments; Analyzed and Interpreted the data.
Yunpeng Zhang, Xin Zhou, Junqiang Xu: Performed the experiments.
Dongbo Mi: Conceived and designed the experiments; Contributed reagents, materials, analysis tools or data; Wrote the paper.

Data availability statement

Data will be made available on request.

Declaration of competing interest

The authors declare no competing financial interest.

Acknowledgement

Appendix A. Supplementary data

Supplementary data to this article can be found online at https://doi.org/10.1016/j.heliyon.2023.e17763.

References

[1] J.K. Lee, D. Samanta, H.G. Nam, R.N. Zare, Micron-sized water droplets induce spontaneous reduction, J. Am. Chem. Soc. 141 (2019) 10585–10589.
[2] Z. Wei, Y. Li, R.G. Cooks, X. Yan, Accelerated reaction kinetics in microdroplets: overview and recent developments, Annu. Rev. Phys. Chem. 71 (2020) 31–51.
[3] C. Gong, D. Li, X. Li, D. Zhang, D. Xing, L. Zhao, X. Yuan, X. Zhang, Spontaneous reduction-induced degradation of viologen compounds in water microdroplets and its inhibition by host-guest complexation, J. Am. Chem. Soc. 144 (2022) 3510–3516.
[4] J.M. Headrick, E.G. Diken, R.S. Walters, N.I. Hammer, R.A. Christie, J. Cui, E.M. Myshakin, M.A. Duncan, M.A. Johnson, K.D. Jordan, Spectral signatures of hydrated proton vibrations in water clusters, Science 308 (2005) 1765–1769.
[5] K.D. Jordan, M.A. Johnson, Downsizing the hydrated electron's pair, Science 329 (2010) 42–43.
[6] M. Zhou, J. Dong, L. Zhang, Q. Qin, Reactions of group V metal atoms with water molecules. Matrix isolation FTIR and quantum chemical studies, J. Am. Chem. Soc. 123 (2001) 135–141.
[7] S. Thurmer, M. Oncak, N. Ottosson, R. Seidel, U. Hergenhahn, S.E. Bradforth, P. Slavicek, B. Winter, On the nature and origin of dicationic, charge-separated species formed in liquid water on X-ray irradiation, Nat. Chem. 5 (2013) 590–596.
[8] D. Mi, K. Chingin, Water radical cations in the gas phase: methods and mechanisms of formation, structure and chemical properties, Molecules 25 (2020) 3490.
[9] M. Kominato, A. Fujii, Infrared spectroscopy of $[H_2O\text{-}X_n]^+$ (n = 1-3, X = N_2, CO_2, CO, and N_2O) radical cation clusters: competition between hydrogen bond and hemibond formation of the water radical cation, Phys. Chem. Chem. Phys. 25 (2023) 14726–14735.
[10] E.P. Lu, P.R. Pan, Y.C. Li, M.K. Tsai, J.L. Kuo, Structural evolution and solvation of the OH radical in ionized water radical cations $(H_2O)_n^{\bullet+}$, n = 5-8, Phys. Chem. Chem. Phys. 16 (2014) 18888–18895.
[11] Q. Cheng, F.A. Evangelista, A.C. Simmonett, Y. Yamaguchi, H.F. Schaefer III, Water dimer radical cation: structures, vibrational frequencies, and energetics, J. Phys. Chem. A 113 (2009) 13779–13789.
[12] O. Svoboda, D. Hollas, M. Oncak, P. Slavicek, Reaction selectivity in an ionized water dimer: nonadiabatic ab initio dynamics simulations, Phys. Chem. Chem. Phys. 15 (2013) 11531–11542.
[13] D. Ben-Amotz, Unveiling electron promiscuity, J. Phys. Chem. Lett. 2 (2011) 1216–1222.
[14] A.J. Lee, S.W. Rick, The effects of charge transfer on the properties of liquid water, J. Chem. Phys. 134 (2011), 184507.
[15] L. Qiu, N.M. Morato, K.H. Huang, R.G. Cooks, Spontaneous water radical cation oxidation at double bonds in microdroplets, Front. Chem. 10 (2022), 903774.
[16] M. Wang, X.-F. Gao, R. Su, P. He, Y.-Y. Cheng, K. Li, D. Mi, X. Zhang, X. Zhang, H. Chen, R.G. Cooks, Abundant production of reactive water radical cations under ambient conditions, CCS Chem 4 (2022) 1224–1231.
[17] D. Mi, Y. Mao, B. Wei, Y.C. Li, X. Dong, K. Chingin, Generation of phenol and molecular hydrogen through catalyst-free C-H activation of benzene by water radical cations, J. Am. Soc. Mass Spectrom. 33 (2022) 68–73.
[18] D. Mi, J. Xu, Y. Zhang, T. Zhu, J. Ouyang, X. Dong, K. Chingin, Formation of protonated water-hydrogen clusters in an ion trap mass spectrometer at room temperature, Phys. Chem. Chem. Phys. 24 (2022) 7180–7184.
[19] G.H. Gardenier, M.A. Johnson, A.B. McCoy, Spectroscopic study of the ion-radical H-bond in $H_4O_2^{\bullet+}$, J. Phys. Chem. A 113 (2009) 4772–4779.
[20] M. Sodupe, A. Oliva, J. Bertran, Theoretical study of the ionization of the $H_2O\text{-}H_2O$, $NH_3\text{-}H_2O$, and $FH\text{-}H_2O$ hydrogen-bonded molecules, J. Am. Chem. Soc. 116 (1994) 8249–8258.
[21] H.M. Lee, K.S. Kim, Water dimer cation: density functional theory vs Ab initio theory, J. Chem. Theor. Comput. 5 (2009) 976–981.
[22] P.A. Pieniazek, J.V. Vondele, P. Jungwirth, A.I. Krylov, S.E. Bradforth, Electronic structure of the water dimer cation, J. Phys. Chem. A 112 (2008) 6159–6170.
[23] L. Angel, A.J. Stace, Dissociation patterns of $(H_2O)^{\bullet+}$ cluster ions, for n=2-6, Chem. Phys. Lett. 345 (2001) 277–281.
[24] M.-F. Lin, N. Singh, S. Liang, M. Mo, J.P.F. Nunes, K. Ledbetter, J. Yang, M. Kozina, S. Weathersby, X. Shen, A.A. Cordones, T.J.A. Wolf, C.D. Pemmaraju, M. Ihme, X.J. Wang, Imaging the short-lived hydroxyl-hydronium pair in ionized liquid water, Science 374 (2021) 92–95.
[25] S.P. de Visser, L.J. de Koning, N.M.M. Nibbering, Reactivity and thermochemical properties of the water dimer radical cation in the gas phase, J. Phys. Chem. 99 (1995) 15444–15447.
[26] S. Yamaguchi, S. Kudoh, Y. Kawai, Y. Okada, T. Orii, K. Takeuchi, Collision reaction of water cluster cations $(H_2O)_n^{\bullet+}$ (n=2 and 3) with D_2O, hem. Phys. Lett. 377 (2003) 37–42.
[27] K. Li, L. Fan, D. Mi, X. Gao, H. Chen, Study on the gas-phase structure of water dimer radical cation using mass spectrometry, J. Chin. Mass Spectrom. Soc. 42 (2021) 1139–1144.
[28] D. Mi, J. Cui, S. Kuang, X. Dong, H. Lu, Facile atmospheric generation of water radical cations via TiO_2-nanoneedle arrays for aromatic hydrocarbon detection based on corona discharge, Bull. Kor. Chem. Soc. 42 (2021) 452–458.
[29] R. March, An introduction to quadrupole ion trap mass spectrometry, J. Mass Spectrom. 32 (1997) 351–369.
[30] de E. Hoffmann, V. Stroobant, Mass Spectrometry: Principles and Applications, John Wiley & Sons, England, 2007.
[31] J. Watson, O. Sparkman, Introduction to Mass Spectrometry: Instrumentation, Applications and Strategies for Data Interpretation, John Wiley & Sons, England, 2007.
[32] A. Good, D.A. Durden, P. Kebarle, Mechanism and rate Constants of ion-molecule reactions leading to formation of $H^+(H_2O)_n$ in moist oxygen and air, J. Chem. Phys. 52 (1970) 222–229.
[33] H. Kambara, Y. Mitsui, I. Kanomata, Identification of clusters produced in an atmospheric pressure ionization process by collision dissociation method, Anal. Chem. 51 (1979) 1447–1452.

[34] K. Mizuse, J.-L. Kuo, A. Fujii, Structural trends of ionized water networks: infrared spectroscopy of watercluster radical cations $(H_2O)_n^{\bullet+}$ (n = 3–11), Chem. Sci. 2 (2011) 868–876.

[35] J.E. McClellan, J.P. Murphy III, J.J. Mulholland, R.A. Yost, Effects of fragile ions on mass resolution and on isolation for tandem mass spectrometry in the quadrupole ion trap mass spectrometer, Anal. Chem. 74 (2002) 402–412.

[36] D. Xing, Y. Meng, X. Yuan, S. Jin, X. Song, R.N. Zare, X. Zhang, Capture of hydroxyl radicals by hydronium cations in water microdroplets, Angew. Chem. Int. Ed. 61 (2022), e202207587.